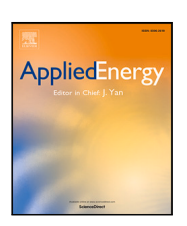
Contents lists available at ScienceDirect

Applied Energy

journal homepage: www.elsevier.com/locate/apenergy





On energy-efficient HVAC operation with Model Predictive Control: A multiple climate zone study

Naren Srivaths Raman¹, Bo Chen, Prabir Barooah *

Department of Mechanical and Aerospace Engineering, University of Florida (MAE-UF), Gainesville, FL 32611, USA

ARTICLE INFO

Keywords:
HVAC control
Model Predictive Control
Energy efficiency
Optimization
Energy system operation
Real-time optimization
Humidity control
Smart building

ABSTRACT

This paper aims to quantify the performance of Model Predictive Control (MPC) for a typical commercial building heating, ventilation and air conditioning (HVAC) system across a wide range of climate and weather conditions. The motivation of the study comes from the fact that although there is a large body of work on MPC for HVAC systems, there is a lack of studies that examine the range of possible performance of MPC, in terms of both energy savings and maintaining indoor climate (temperature and humidity) as a function of outdoor weather. A challenge in conducting such a study is developing an MPC controller that can be used in a wide range of weather. The root cause of this challenge is the need for a tractable cooling and dehumidification coil model that can be used by the MPC controller, since the coil may operate in quite distinct modes depending on weather. We present such an MPC controller, and then leverage it to conduct an extensive simulation campaign for fourteen climate zones in the United States and four weather conditions (winter, spring, summer, and fall) in each climate zone. The performance of the proposed controller is compared with not only a rule-based baseline controller but also with a simpler MPC controller that ignores humidity and latent heat considerations. There are several results the arise from this comparative study. One such result is that energy savings from MPC over baseline can vary dramatically based on climate and season. Another is that the effect of ignoring humidity in the MPC formulation can lead to poor indoor humidity control more in milder weather rather than in hot weather. The results from this study can help practitioners and researchers assess costs and benefits of proposed MPC formulations for HVAC control.

1. Introduction

Model predictive control (MPC) for heating, ventilation, and air conditioning (HVAC) systems in commercial buildings for energy efficiency improvement has been an active area of research; see the review papers [1,2]. One of the reasons for the interest in MPC is the high energy consumption of HVAC systems, and a recognition that an advanced control algorithm can be a cost-effective way to reduce their energy use. In MPC, at every time instant control commands are decided by solving an optimization problem over a finite planning horizon into the future, implementing only the first segment of the plan, and then repeating the process ad infinitum. In case of building climate control, the advantage of MPC is that it can explicitly take into account competing requirements such as reducing energy use while maintaining indoor climate variables within allowable ranges.

Many distinct MPC schemes have been proposed in the context of energy efficient HVAC operation, differing in the type of HVAC system considered, the objective function to minimize, types of models used as constraints by the optimizer, etc. Each study, whether simulation-based or experimental, uses a different HVAC system configuration, outdoor weather, and optimization problem formulation. The effect of outdoor weather can be particularly strong. In experimental studies, outdoor weather cannot be varied beyond what is observed at the location of the test.

A gap in the existing literature on MPC for energy efficient HVAC operation is the lack of information on the range of performance that MPC can exhibit for a wide range of outdoor weather conditions. Here performance includes both energy savings and indoor climate (temperature and humidity). To the best of our knowledge, the only work that studies energy savings potential of HVAC control algorithms over a large number of climate zones is [3], but the controllers tested in that paper are rule-based, not MPC.

E-mail addresses: narensraman@ufl.edu (N.S. Raman), bo.chen@ufl.edu (B. Chen), pbarooah@ufl.edu (P. Barooah).

This research reported here has been partially supported by the National Science Foundation, USA through award # 1463316 and the State of Florida through a REET (Renewable Energy and Energy Efficiency Technologies) grant.

^{*} Corresponding author

 $^{^{1}\,}$ Raman was with MAE-UF during the period in which the work was done.

Nomenclature

R

 r_{oa}

 \mathbb{R}

RH

COP Coefficient of performance

E Energy

hSpecific enthalpyNPlanning horizon n_p Number of personsPPower (electrical)qPower (thermal)

 $q_{\it other}$ Rate of heat generated by people etc. inside

the building Resistance Outdoor air ratio Relative humidity

T Temperature (dry bulb, if air)

 $\begin{array}{lll} u & & \text{Control command} \\ V_H & & \text{Humidity violation} \\ V_T & & \text{Temperature violation} \\ W & & \text{Humidity ratio} \\ w & & \text{Disturbance} \end{array}$

State

 Δt Sampling period η Efficiency η_{sol} Solar irradiance λ Weights

 ω Water vapor generation rate

 ω_{other} Rate of moisture generated by people etc.

inside the building Set of real numbers

Slack variable

bp Building pressurization

Occupied mode occ Unoccupied mode unocc Conditioned air caCooling coil ccDrv air da ia Indoor air j, kTime index ma Mixed air oa Outdoor air pha Pre heat air Return air raReheat air rhaSupply air sa Water w Water at inlet wi

This paper addresses the aforementioned gap by conducting an extensive simulation campaign with two distinct MPC controllers applied to an HVAC system, for fourteen distinct climate zones – for all the states and territories of the United States – and for four seasons (winter, spring, summer, and fall) in each climate zone. Though limited to one country, these $14 \times 4 = 56$ scenarios span a wide range of outdoor weather conditions seen in many parts of the world.

Water at outlet

The HVAC system used for the study is a single duct variable air volume hydronic system with pre-heat, cooling and dehumidification, and reheat coils (see Fig. 1). This configuration is common in medium and large commercial buildings across the USA.

This paper makes three contributions to the existing literature on MPC for HVAC systems. The first contribution is that the study provides a preliminary answer to the question: in which climate zones MPC is likely to provide significant energy savings and thermal comfort performance to be competitive with simpler rule-based controllers that are currently in use? While a decision by a building owner to invest in MPC will require a study specifically designed for the building in question, this study can be used as a preliminary guide.

To describe the second contribution, we have to first describe the challenge in designing an MPC controller that can be used in a wide range of weather conditions without making it computationally intractable or requiring a human expert to redesign the controller for that weather. A large subset of MPC formulations in the literature ignore humidity and latent heat, focusing only on the (dry bulb) space temperature. The inclusion of moisture makes the problem considerably more challenging, primarily since a model of the cooling and dehumidifying coil is needed. The heat transfer and condensation (moisture removal) process on the coil surface is highly complex and difficult to model. In addition, the model must be simple, since MPC uses the model as a constraint in an optimization problem that has to be solved in real time. A complicated model will increase the computational complexity of the optimization problem, potentially rendering it unusable. Such a control-oriented dehumidification coil model was described in our prior work [4] which was used successfully to perform MPC simulations for hot-humid weather. However, this simplified model was not accurate enough for all climate zones. To obtain a high prediction accuracy while keeping the same model structure, a sequence of models, each parameterized by certain coil inlet conditions, can be used. But doing so leads to a high-dimensional mixed-integer nonlinear program (MINLP), with integer variables corresponding to which model among the set of models is to be used at any given time instant. Such MINLPs are nearly impossible to solve in a real-time setting.

In this paper we use a reformulation of the optimization problem that retains the non-linear program (NLP) nature of the optimization problem without any integer-valued variables. NLPs are far easier to solve than mixed integer problems. In fact, simulations show that the real-time computational cost of the proposed MPC controller is quite low. The proposed MPC formulation, which we call WISL-MPC here (for Weather-Independent-Sensible-Latent-MPC), was introduced in our preliminary work [5], but it was tested only for two specific climate zones and seasons in that study. The simulations presented in this paper verifies the claim that the proposed MPC scheme can be indeed used in a wide range of climate zones without either having to solve a high dimensional MINLP or having to retune the MPC formulation by a human expert depending on the climate. This is the second contribution of the paper.

The third contribution is the comparison between the proposed WISL-MPC controller - that takes into account latent heat balance and humidity constraints explicitly in the optimization problem - and another MPC controller (S-MPC, from [4]) - that only considers sensible heat balance and temperature constraints but ignores latent heat balance and humidity constraints. The S-MPC scheme is representative of the majority of MPC schemes proposed in the literature and studied in experimental demonstrations. The WISL-MPC controller is more expensive than S-MPC: both real-time computation and the modeling effort required are higher for WISL-MPC. On the other hand, S-MPC may lead to poor humidity control and thus poor thermal comfort and even mold growth [6]. So a natural question arises: when is the extra cost of WISL-MPC warranted, and when can one deploy the less expensive S-MPC scheme? The simulation study presented here provides an answer to this question as well, since it compares the performance of both the MPC schemes in every climate zone and season. Somewhat surprisingly,

S-MPC – which ignores humidity and latent heat – successfully provides humidity control in hot-humid climates during peak summer but fails to meet humidity requirements in milder weather in the same climate zone. More generally, *S-MPC* leads to humidity violations in moist and marine climates. Both the MPC controllers provide similar performance in dry climates.

Overall, it is found that WISL-MPC provides significant amount of energy savings over the baseline controller, and is able to maintain the thermal comfort constraints as well or better than the baseline controller. The energy savings vary considerably by climate zone and weather. The humidity-agnostic MPC controller, S-MPC, provides nearly the same amount of energy savings as the WISL-MPC controller in many scenarios, but it often causes poor humidity control, especially in moist climate zones and in mild seasons. These results validate the need for incorporating humidity and latent heat in MPC, as well as the need for a study of MPC performance as a function of climate zone.

The baseline controller used in the study is the so called Dual Maximum controller [7]. The Single Maximum controller is in fact more widely used in practice than the Dual Maximum controller, but Dual Maximum is more energy efficient [7,8]. So the actual savings with WISL-MPC in practice are likely to be higher than those reported.

The rest of the paper is organized as follows. Section 1.1 provides a detailed review of relevant literature, including a description of the contribution over our own prior works [4,5] that this paper is an extension of. Section 2 describes the HVAC system under study. Section 3 describes the two MPC schemes and the baseline controller. Section 4 describes the simulation setup, and Section 5 describes the simulation results. Section 6 makes concluding remarks.

1.1. Review of prior work, and contributions

Since the aim of this paper is to study the effect of weather spanning many climate zones, including hot and humid climates, on MPC performance, and both humidity and temperatures are important metrics for performance, we limit our review to those papers on HVAC MPC that have considered at least humidity if not both humidity and latent heat.

Based on the objective function to be minimized, a MPC formulation can be classified into (i) economic MPC and (ii) set point tracking MPC [9]. In set point tracking MPC, the objective function is typically a deviation from the setpoint, so that minimizing would drive the relevant output(s) to the desired set point(s). In economic MPC, the objective function can be any performance measure, not necessarily deviation from setpoints.

The MPC controllers studied in this paper, and those in Refs. [8,10-19] belong to the economic MPC category. In [17], it is assumed that the relative humidity of the conditioned air after the cooling coil is always 100%. In [10], this value is assumed to be always 90%, while [8] assumes both the temperature and the humidity ratio of the conditioned air are constant. These assumptions avoid the need for modeling the cooling and dehumidification process at the coil, though the validity of these assumptions is questionable. Such simplifying assumptions are not made in this paper. An economic MPC scheme for energy use minimization with humidity and latent heat considerations is presented in [12]. Unlike the hydronic system used in this work, the focus in [12] is on direct expansion systems. MPC is used to control a variable refrigerant flow HVAC system in [13]. In [14], space humidity is controlled using a proportional-integral controller, but humidity is not considered directly in their MPC formulation while it is in this paper.

In [15], MPC is used to control an environmental chamber located at the Pennsylvania State University campus. Latent heat is ignored in the MPC formulation, though humidity is indirectly considered through a data-driven thermal comfort model. In [18], a token based scheduling algorithm is used to minimize the energy consumption for a building located at the Nanyang Technological University, Singapore. Humidity constraint is incorporated through a thermal sensation model used but

latent heat is ignored. In contrast to [15,18], latent heat is directly considered here. An enthalpy control algorithm is used in [16] to regulate the amount of outdoor air supplied to a building. Several more commands – in addition to outdoor air – are decided by the controller in this paper.

A few works have used a hybrid between economic and setpoint MPC: the objective function consist of both energy use and deviation from set point terms, e.g. [20–22]. Multiple MPC strategies are compared for an air handling unit in [20]. It is assumed that the temperature and humidity ratio after the cooling coil can be chosen independently, thereby eliminating the need for a cooling coil model. This assumption will not hold in reality, since only inlet conditions of the coil can be independently manipulated. Unlike the cooling-based air dehumidification considered in this work, Ref. [21] uses a liquid desiccant system for cooling and dehumidification.

Ref. [22] is more relevant to our work; they use a cooling coil model in their optimization. Temperature and humidity of the conditioned air are modeled correctly as coupled. Unlike our formulation, the supply air flow rate is not a control command in [22]. The MPC optimizer in [22] uses short prediction horizon of 10 min, so it cannot plan for disturbances in longer time scales. In contrast, we use a prediction horizon of 24 h. Genetic algorithm (GA) is used in [22] to perform the minimization involved in computing control commands. Nondeterministic optimization algorithms such as GA are challenging for real-time computation. In contrast, we use a deterministic search method through a nonlinear programming (NLP) solver.

MPC works that report experimental evaluations in real buildings are of special interest even if they do not consider humidity and latent heat in their MPC formulation. After all, if an MPC controller - irrespective of the optimization formulation - can maintain temperature and humidity constraints in real buildings while saving energy, then incorporating humidity related features into the controller-which necessarily increases complexity—is perhaps not necessary. In particular, Refs. [23-26] describe experimental demonstrations that have been carried out with MPC-based controllers on real buildings. The problem formulations in [23-25] do not consider latent heat and humidity, and they do not report humidity measurements. Ref. [26] reports a simplified comfort index that is based on measurements of humidity and temperature, which shows comfort constraints are maintained in their experiments, but these experimental results for a specific building in Singapore. Our focus is to study MPC under a wide range of climate and weather conditions.

Our previous work [4] addressed the problem of incorporating latent heat and humidity by developing a reduced order cooling and dehumidification coil model that was used as a constraint in the MPC optimization. As discussed above, the model was not suitable for all climate zones, and a straightforward extension with a bank of models, each suitable for a range of coil inlet conditions, would lead to an intractable high dimensional MINLP. A workaround was proposed in [5] that avoided the need for MINLP, but kept the optimization as an NLP.

The contributions of this paper over our preliminary study [5] are twofold. The study [5] tested the MPC formulation only on two climate zones: hot-humid and hot-dry, and thus did not establish that the proposed controller can indeed be applied to a wide range of outdoor weather conditions successfully without requiring a redesign by a human expert. This paper establishes that claim by applying it to 14 distinct climate zones that covers the contiguous USA (i.e., the lower 48 states), Alaska and Puerto Rico, Guam and Hawaii. In each climate zone, weather from four different seasons are used for simulations. Together, these 56 combinations represent a wide range of outdoor weather conditions. The proposed WISL-MPC controller is seen to perform well in all of these scenarios. Second, the poor performance of the MPC formulation that ignores latent heat in many climate zones is seen in this study for the first time. Finally, many details were omitted in [5], which are described here to make the presentation self contained.

2. System description

We consider a single-zone variable-air-volume hydronic HVAC system, whose schematic is shown in Fig. 1. Throughout the manuscript, the subscripts ma, pha, ca, and sa are used to denote the four locations indicated in Fig. 1: ma stands for $mixed\ air$ (before the preheating coil), pha stands for $preheat\ air$ (between the preheating and the cooling coils), ca stands for $conditioned\ air$ (between the cooling coil and the reheating coil), and ca stands for ca stands for

In such a system, part of the air supplied to the building is recirculated and mixed with fresh outdoor air. If this mixture is too cold, it is heated at the preheating coil so that the downstream cooling coil is protected from freezing and bursting. This air is sent through the cooling and dehumidification coil, thereby reaching conditioned air temperature (T_{ca}) and humidity ratio (W_{ca}) after the coil. If the air before the cooling coil is dry, then there is only cooling but no dehumidification, i.e., $T_{ca} \leq T_{pha}$ and $W_{ca} = W_{pha}$. The conditioned air is typically quite cold and is therefore reheated at the reheating coil to the supply air temperature (T_{sa}) and finally supplied to the zone. There is no phase change of the moisture in the air (water vapor \leftrightarrow water) across the reheating or preheating coils, so the humidity ratio of the supply air is the same as the conditioned air ($W_{sa} = W_{ca}$), and the humidity ratio of the preheated air is the same as the mixed air ($W_{pha} = W_{ma}$).

The configuration shown in Fig. 1 is quite common in commercial buildings in the continental U.S. The reason is reliability under extreme conditions that are not uncommon. Even in typically cold climates such as that in Chicago, Illinois, hot-humid weather occurs in the summer, requiring the cooling and dehumidification coil and thus the reheating coil. Similarly, in many warm-humid climates extremely cold weather occurs on certain winter days; such as Gainesville, Florida. That necessitates the preheating coil, since otherwise the cooling coil can freeze and burst, causing expensive disruption. Thus, a minimal requirement for a climate-independent HVAC control algorithm is that is must be applicable to the configuration shown in Fig. 1.

The role of an HVAC control system is to maintain thermal comfort and indoor air quality by varying control commands. In the HVAC system shown in Fig. 1, the following commands can be manipulated by the controller:

- (1) supply air flow rate (m_{sa}) ,
- (2) outdoor air ratio ($r_{oa}:=\frac{m_{oa}}{m_{sa}}=\frac{m_{oa}}{m_{oa}+m_{ra}}$, where m_{oa} and m_{ra} are the flow rates of outdoor air and return air, respectively),
- (3) preheated air temperature (T_{pha}) ,
- (4) conditioned air temperature (T_{cq}) , and
- (5) supply air temperature (T_{sa}) .

So the control command vector is:

$$u := [m_{sa}, r_{oa}, T_{ca}, T_{sa}, T_{pha}]^T \in \mathbb{R}^5$$
 (1)

These five control commands are sent as set points to low-level control loops comprised of proportional-integral (PI) controllers.

2.1. Virtual building (VB) simulator

To avoid confusion between the model the MPC controller uses for making decisions, which is simpler than the model used to simulate the HVAC system, the latter will be referred to as the "virtual building" (VB) in the sequel. The overall virtual building consists of hygrothermal dynamics of a single-zone building coupled with a model of the cooling coil, heating coil, and preheating coil. The virtual building is of the form $x(k+1) = f\left(x(k), u(k), w(k)\right)$, where x is the state vector, u is the control command vector, and w is the exogenous input (disturbance) vector. The state vector consists of indoor (dry bulb) air temperature (T_{ia}) , wall temperature (T_{wall}) , indoor air humidity ratio (W_{ia}) , and conditioned air humidity ratio (W_{ca}) , i.e., $x := [T_{ia}, T_{wall}, W_{ia}, W_{ca}]^T \in$

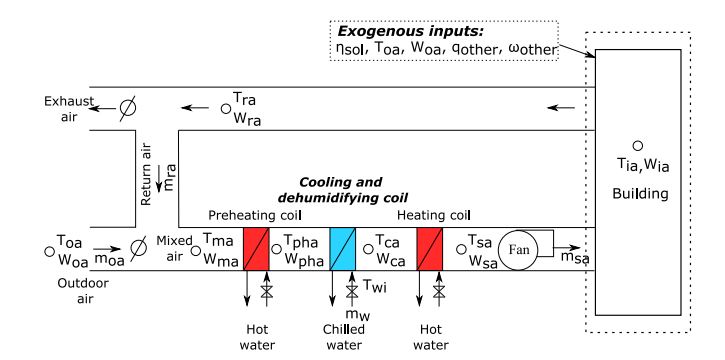


Fig. 1. Schematic of a single-zone variable-air-volume hydronic HVAC system.

 \mathbb{R}^4 . The control command vector u is defined in (1). The exogenous input vector consists of solar irradiance (η_{sol}) , outdoor air temperature (T_{oa}) , outdoor air humidity ratio (W_{oa}) , internal heat load (q_{other}) due to occupants, lights, equipments, etc., and rate of internal water vapor generation (ω_{other}) due to occupants, equipments, etc. Therefore, $w := [\eta_{sol}, T_{oa}, W_{oa}, q_{other}, \omega_{other}]^T \in \mathbb{R}^5$.

The parameters of virtual building – the combined hygrothermal model and cooling coil model – are chosen to mimic a real building and its HVAC system; a 465 m^2 (5000 sq.ft.) auditorium in Pugh Hall located at the University of Florida campus which is served by an air handling unit that has the same configuration as shown in Fig. 1.

2.1.1. Hygrothermal model in the VB

The hygrothermal model is a discretized form of a coupled ordinary differential equation (ODE) model with three states. Two of the ODEs correspond to the two temperature states of a resistance–capacitance (RC) network model, specifically, a 2R2C model. The third ODE corresponds to the zone humidity state, which is affected by the zone temperature. The parameters of the RC-network (temperature) submodel were obtained by fitting the model to measured data from the Pugh Hall auditorium mentioned above. The reader interested in the details of the model and the parameter fitting method used is referred to [27]. Details of the humidity dynamic model can be found in [28]. The only parameter in the humidity sub-model is the volume of the zone.

Inputs to the hygrothermal model include the conditioned air temperature and flow rate, which are outputs of the cooling coil model (described next), thereby coupling the two models to create the virtual building simulator.

2.1.2. Cooling and dehumidifying coil model in the VB

The cooling and dehumidification coil model strongly informs the proposed MPC formulation. The interested readers are referred to our prior work [4] for a detailed description of the cooling coil model and how its parameters are fitted; here we describe it briefly. The cooling coil model is a gray box data-driven model which was developed in [29]. The model consists of five inputs and two outputs; see Fig. 2. The inputs are: (i) supply airflow rate (m_{sa}) , (ii) preheated air temperature (T_{pha}) , (iii) preheated air humidity ratio (W_{pha}) , (iv) chilled water flow rate (m_w) , and (v) inlet water temperature (T_{wi}) . The outputs are conditioned air temperature (T_{ca}) and humidity ratio (W_{ca}) . The parameters of this model are fitted using data obtained from Energy-Plus [30]. The EnergyPlus model is constructed by using manufacturer's information on the coil used in Pugh Hall.

It was observed during modeling that for a *fixed* mixed temperature and relative humidity of the air entering the coil, the outputs T_{ca} and W_{ca} can be predicted quite well by a 5th degree polynomial function of the remaining inputs, namely, the mass flow rates of chilled water and supply air. Fig. 3 shows an example of such predictions. A single polynomial, however, leads to large errors when used at different

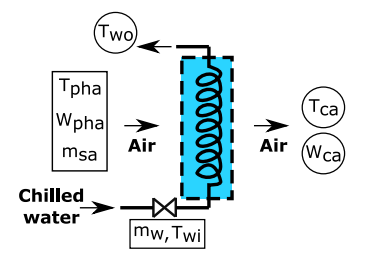
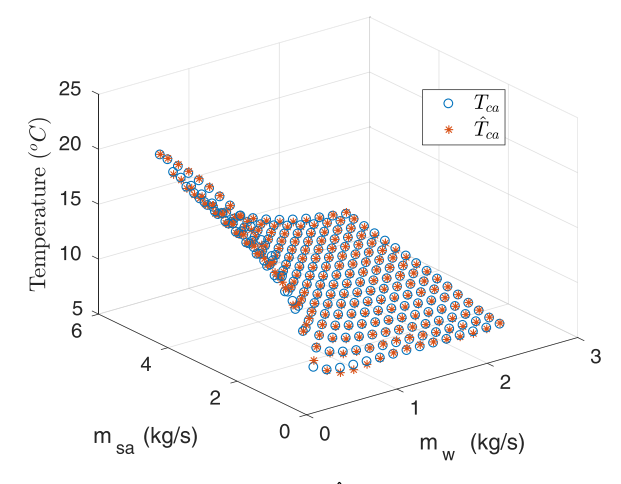
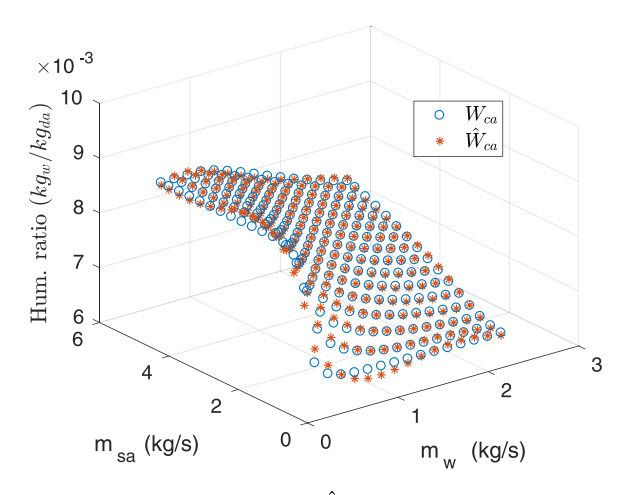


Fig. 2. Schematic of a cooling coil: model inputs in rectangles, and outputs in circles.



(a) Measured (T_{ca}) and predicted (\hat{T}_{ca}) value of conditioned air temperature for a specific bin, $T_{pha}=23.9~^{\circ}C$ (75 $^{\circ}F$) and $RH_{pha}=50\%$. "Measured" refers to data collected from an EnergyPlus simulation.



(b) Measured (W_{ca}) and predicted (\hat{W}_{ca}) value of conditioned air humidity ratio for a specific bin, $T_{pha}=23.9~^{\circ}C$ (75 $^{\circ}F$) and $RH_{pha}=50\%$. "Measured" refers to data collected from an EnergyPlus simulation.

Fig. 3. A slice of the predictions from the cooling coil model used in the virtual building

mixed air temperatures and relative humidities. We therefore used a bank of such polynomials, by first binning the inputs according to T_{pha} and RH_{pha} into 1159 bins, and then fitting the parameters of the polynomial for each bin. The resulting model is called a "binned model". During simulation, given the current coil inlet air conditions, the right polynomial from this bank of polynomials is picked, and then used to predict coil outlet conditions based on the flow rates of chilled water and mixed air.

3. Control algorithms

In this section, we describe three control algorithms: (i) the proposed MPC controller that incorporates humidity and latent heat, called WISL-MPC (for Weather-Independent-Sensible-Latent-MPC), (ii) an MPC controller that considers only sensible heat, called S-MPC (for Sensible-Only-MPC), and (iii) a rule-based controller that serves as the baseline (BL). All three controllers need to decide the same five control commands defined in (1). The underlying optimization problems in both the MPC controllers are nonconvex, but always feasible due to the use of slack variables.

The focus of this paper is energy efficiency, and the total energy consumed over a time duration $[j\Delta t, (j+N)\Delta t]$, where Δt is the sampling period, is:

$$\Delta t \sum_{k=j}^{j+N-1} P_{total}(k) \tag{2}$$

where $P_{total}(k)$ is the total power consumption of the HVAC system at the kth time instant, meaning, during $[k (k+1)]\Delta t$:

$$P_{total}(k) := P_{fan}(k) + P_{preheat}(k) + P_{cc}(k) + P_{reheat}(k).$$
(3)

 P_{fan} is the fan power consumption [31]:

$$P_{fan}(k) = \alpha_{fan} m_{sa}(k)^2. \tag{4}$$

The cooling and dehumidifying coil power consumption P_{cc} is proportional to the heat it extracts from the preheated air stream as follows:

$$P_{cc}(k) = \frac{m_{sa}(k)[h_{pha}(k) - h_{ca}(k)]}{\eta_{cc}COP_c},$$
(5)

where h_{pha} and h_{ca} are the specific enthalpies of the preheated air and conditioned air respectively. We refer the interested reader to [4] for details about the enthalpy terms and the efficiency and coefficient of performance (η_{cc} and COP_c).

Recall that there is no change in the humidity ratio across the preheating or reheating coils. Therefore, their power consumptions depend only on the temperatures before and after the coils and not on humidities. The preheating and reheating coil power consumptions $P_{preheat}$ are modeled as the heat they add to their respective air streams with efficiency factors and boiler COPs:

$$P_{preheat}(k) = \frac{m_{sa}(k)C_{pa}[T_{pha}(k) - T_{ma}(k)]}{\eta_{preheat}COP_h},$$
(6)

$$P_{preheat}(k) = \frac{m_{sa}(k)C_{pa}[T_{pha}(k) - T_{ma}(k)]}{\eta_{preheat}COP_h},$$

$$P_{reheat}(k) = \frac{m_{sa}(k)C_{pa}[T_{sa}(k) - T_{ca}(k)]}{\eta_{reheat}COP_h}.$$
(6)

weather-independent 3.1. Proposed model predictive controller (WISL-MPC)

Fig. 4 shows the control architecture for the proposed WISL-MPC controller.

The decision variables in the optimization problem underlying the proposed MPC controller consists of the following: (i) the states of the process $x(k) := [T_{ig}(k), W_{ig}(k)]^T \in \mathbb{R}^2$, (ii) the vector of control commands and internal variables $v(k) := [u(k)^T, m_{w,T}(k), m_{w,W}(k), W_{cq}(k)]^T$ $\in \mathbb{R}^8$, where u(k) is the control command vector defined in (1), and $m_{w,T}(k), m_{w,W}(k)$ are fictitious cooling coil water flow rate variables that will be described in Section 3.1.1, and (iii) the vector of nonnegative slack variables $\zeta(k) := [\zeta_T^{low}(k), \zeta_T^{high}(k), \zeta_W^{low}(k), \zeta_W^{high}(k), \zeta_{m_w}(k)] \in \mathbb{R}^5$ which are introduced for feasibility. The controller needs forecast of the exogenous input vector $w(k) \in \mathbb{R}^5$ (defined earlier) over the planning horizon N.

In simulations reported later, we use $\Delta t = 10$ minutes and planning horizon N = 144, corresponding to 24 h. Therefore, there are 2160 (= 144×{2 +8 +5}) decision variables. Mathematically the optimization

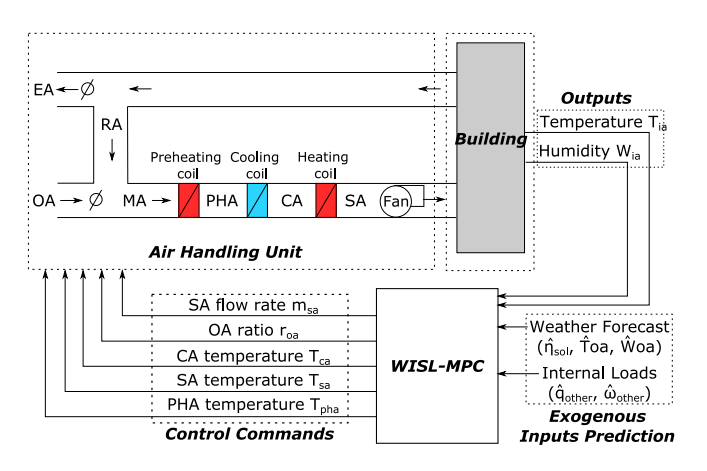


Fig. 4. *WISL-MPC*, control architecture. In this figure, OA: outdoor air, EA: exhaust air, RA: return air, MA: mixed air, PHA: preheated air, CA: conditioned air, and SA: supply air.

problem at time index *j* consists of the following minimization (subject to constraints that will be described soon):

$$\min_{V,X,Z} \sum_{k=j}^{j+N-1} \left[P_{fan}(k) + P_{cc}(k) + P_{reheat}(k) + \lambda_{preheat} P_{preheat}(k) + P_{slack}(k) \right] \Delta t, \tag{8a}$$

where V,X,Z are tall vectors obtained by stacking together $v(k),x(k),\zeta(k)$'s over the planning horizon, and $P_{fan},P_{cc}^{SL},P_{reheat}$, and $P_{preheat}$ are given by (4), (5), (7), and (6) respectively. The last term, P_{slack} , penalizes the zone temperature, zone humidity, and chilled water flow rate slack variables:

$$\begin{split} P_{slack}(k) &:= \lambda_T^{low} \zeta_T^{low}(k) + \lambda_T^{high} \zeta_T^{high}(k) \\ &+ \lambda_W^{low} \zeta_W^{low}(k) + \lambda_W^{high} \zeta_W^{high}(k) + \lambda_{m_w} \zeta_{m_w}(k), \end{split}$$

where the λs are penalty parameters. The minimization (8a) together with the following constraints define the MPC optimization problem at time i:

$$\begin{split} T_{ia}(k+1) &= T_{ia}(k) + \frac{\Delta t}{C} \left[\frac{(T_{oa}(k) - T_{ia}(k))}{R} + q_{\text{HVAC}}(k) \right. \\ &\left. + A_e \eta_{sol}(k) + q_{other}(k) \right] \end{split} \tag{8b}$$

$$q_{\text{HVAC}}(k) = m_{sa}(k)C_{pa}(T_{sa}(k) - T_{ia}(k))$$
 (8c)

$$W_{ia}(k+1) = W_{ia}(k) + \frac{\Delta t R_g T_{ia}(k)}{V P^{da}} \left[\omega_{other}(k) + m_{sa}(k) \frac{W_{sa}(k) - W_{ia}(k)}{1 + W_{sa}(k)} \right]$$
(8d)

$$T_{ca}(k) = f_{co}(T_{pha}(k), W_{pha}(k), m_{sa}(k), m_{w,T}(k))$$
 (8e)

$$W_{ca}(k) = g_{co}(T_{pha}(k), W_{pha}(k), m_{sa}(k), m_{w,W}(k))$$
(8f)

$$m_{w,W}(k) = m_{w,T}(k) - \zeta_{m_w}(k)$$
 (8g)

$$\begin{split} T_{ia}^{low}(k) - \zeta_T^{low}(k) &\leq T_{ia}(k) \leq T_{ia}^{high}(k) + \zeta_T^{high}(k) \\ a^{low}T_{ia}(k) + b^{low} - \zeta_W^{low}(k) &\leq W_{ia}(k) \end{split} \tag{8h}$$

$$\leq a^{high}T_{ia}(k) + b^{high} + \zeta_W^{high}(k) \tag{8i}$$

$$\max(m_{sa}(k) - m_{sa}^{rate} \Delta t, m_{sa}^{low}) \le m_{sa}(k+1)$$

$$\le \min(m_{sa}(k) + m_{sa}^{rate} \Delta t, m_{sa}^{high})$$
(8j)

$$\max \left(T_{pha}(k) - T_{pha}^{rate} \Delta t, T_{pha}^{low}, T_{ma}(k+1) \right) \le T_{pha}(k+1)$$

$$\le \min_{k \in \mathbb{N}} \left(T_{pha}(k) + T_{pha}^{rate} \Delta t, T_{pha}^{high} \right)$$

$$\leq \min \left(T_{pha}(k) + T_{pha}^{rate} \Delta t, T_{pha}^{high} \right) \tag{8k}$$

$$\max(r_{oa}(k) - r_{oa}^{rate} \Delta t, r_{oa}^{low}) \le r_{oa}(k+1)$$

$$\leq \min\left(r_{oa}(k) + r_{oa}^{rate} \Delta t, r_{oa}^{high}\right) \tag{81}$$

 $\max(T_{ca}(k) - T_{ca}^{rate} \Delta t, T_{ca}^{low}) \le T_{ca}(k+1)$

$$\leq \min\left(T_{ca}(k) + T_{ca}^{rate} \Delta t, T_{pha}(k+1)\right) \tag{8m}$$

 $\max \left(T_{sa}(k) - T_{sa}^{rate} \Delta t, T_{ca}(k+1)\right) \le T_{sa}(k+1)$

$$\leq \min\left(T_{sa}(k) + T_{sa}^{rate}\Delta t, T_{sa}^{high}\right) \tag{8n}$$

$$W_{ca}(k) \le W_{pha}(k) \tag{80}$$

$$\zeta_T^{low}(k+1), \ \zeta_T^{high}(k+1) \ge 0$$
 (8p)

$$\zeta_{W}^{low}(k+1), \ \zeta_{W}^{high}(k+1), \ \zeta_{m...}(k) \ge 0$$
 (8q)

where constraints (8b)–(8g) and (8o)–(8q) are for k = j, ..., j + N - 1, constraints (8h) and (8i) are for k = j + 1, ..., j + N, and constraints (8j)–(8n) are for k = j - 1, ..., j + N - 2.

Note that the cooling coil power consumption $P_{cc}(k)$ used in the objective function (8a) is given by (5) which is a function of enthalpy and thus accounts for both sensible and latent heat transfers.

Constraints (8b) and (8d) are for the discretized temperature and humidity dynamics model of the indoor air, respectively. The temperature model (8b) is a discretized form of a 1st order resistor–capacitor model, with R,C being thermal resistance and capacitance of the building, and $q_{\rm HVAC}$ is the heat influx into the building due to the HVAC system's action. The continuous-time version of humidity dynamics (8d) is derived in [28], where V is the air volume of the building, R_g is the specific gas constant of dry air, P^{da} is the partial pressure of dry air.

Constraints (8e), (8f), and (8g) are for the control-oriented cooling coil model which is presented in the next subsection (Section 3.1.1).

Constraints (8h) and (8i) are box constraints to maintain temperature and humidity of the zone within the allowed comfort limits. Usually the limits during the unoccupied mode are more relaxed than the occupied mode, i.e., $[T_{ia}^{low,occ}, T_{ia}^{high,occ}] \subseteq [T_{ia}^{low,unocc}, T_{ia}^{high,unocc}]$ and $[RH_z^{low,occ}, RH_z^{high,occ}] \subseteq [RH_z^{low,unocc}, RH_z^{high,unocc}]$, as shown in Fig. 10. RH_z is the relative humidity of the zone, which is a highly nonlinear function of dry bulb temperature and humidity ratio [32, Chapter 1]. We linearize this function which gives us the coefficients a^{low} , b^{low} , a^{high} , and b^{high} in (8i), and thus form convex sets, as shown in Fig. 10.

Constraint (8j) accounts for the capability of the fan. The minimum supply airflow rate is computed based on the ventilation requirements specified by ASHRAE 62.1 [33] and to maintain positive building pressurization.

Constraints (8k)–(8n) account for the capabilities of the preheating coil, damper actuators, cooling coil, and reheating coil. In constraints (8k) and (8n), the inequalities $T_{pha}(k+1) \ge T_{ma}(k+1)$ and $T_{sa}(k+1) \ge T_{ca}(k+1)$ ensure that the preheating and reheating coils can only add heat; they cannot cool the air. Similarly, in constraints (8m) and (8o), the inequalities $T_{ca}(k+1) \le T_{pha}(k+1)$ and $W_{ca}(k+1) \le W_{pha}(k+1)$ ensure that the cooling coil can only cool and dehumidify the air stream; it cannot add heat or moisture. Inequality constraints (8p) and (8q) ensure that the slack variables are nonnegative.

Even though the temperature dynamics used in the optimization problem are linear, the humidity dynamics – which form part of the constraints – are nonlinear, which make the optimization problem nonconvex. Some of the terms in the objective function are nonconvex as well.

3.1.1. Control-oriented cooling coil model used in WISL-MPC

Constraints (8e), (8f), and (8g) are for the control-oriented cooling coil model, which is a modified version of the model developed in [4]. Fig. 2 shows all the relevant variables (inputs and outputs) of a cooling and dehumidification coil model. First we describe the control oriented model proposed in [4], before discussing the modifications needed to make the MPC formulation climate/weather independent. The model proposed in [4] is

$$T_{ca}(k) = T_{pha}(k) +$$

$$\begin{split} m_w(k) \; f_{cc} \left(T_{pha}(k), W_{pha}(k), m_{sa}(k), m_w(k) \right) \\ W_{ca}(k) &= W_{pha}(k) + \end{split} \tag{9}$$

$$m_w(k) g_{cc}(T_{pha}(k), W_{pha}(k), m_{sa}(k), m_w(k))$$
 (10)

where m_w is the chilled water flow rate. Note that when the chilled water flow rate is zero, no cooling or dehumidifying of the air occurs. That is, when $m_w=0$ the conditioned air temperature and humidity ratio must be equal to the preheated air temperature and humidity ratio: $T_{ca}=T_{pha}$ and $W_{ca}=W_{pha}$. The form of the right hand sides of (9)–(10) were chosen make the model exhibit this behavior. The functions f and g are chosen as quadratic in their arguments; higher degree polynomials did not show substantial gain in accuracy. The validation reported in [4] showed that the maximum prediction errors observed are 1.61 °C (3 °F) and $1.1 \times 10^{-3}~{\rm kg_w/kg_{da}}$ for T_{ca} and W_{ca} , respectively.

Depending on the condition of the preheat air and other inputs, one of three scenarios can occur: (i) neither cooling nor dehumidification occurs ($T_{ca} = T_{pha}$ and $W_{ca} = W_{pha}$), (ii) both cooling and dehumidification occurs ($T_{ca} \leq T_{pha}$ and $W_{ca} \leq W_{pha}$), and (iii) only cooling but no dehumidification occurs ($T_{ca} \leq T_{pha}$ and $W_{ca} = W_{pha}$). The first situation is handled by the model well since it occurs only when $m_w = 0$, and by design the model predicts that behavior. It turns out that the second situation is also predicted reasonably well by the model.

However, the third situation occurs in the extreme range of the input values of the model: when the preheated air is quite dry but also quite hot. No matter how much chilled water is supplied the coil can only cool down the air but cannot dehumidify it further. Due to the simple structure of the model, it is unable to predict that situation well. Instead, the model—when fitted to reduce the overall prediction error—might predict that the air is humidified further as it moves across the coil, which is physically impossible, and furthermore, conflicts with the constraint (80) that is imposed precisely to prevent such behavior.

To improve predictions of the model in the third scenario without having to switch among a set of models, we split the chilled water flow rate m_w into two fictitious variables $m_{w,T}$ and $m_{w,W}$:

$$T_{ca}(k) = T_{pha}(k) +$$

$$m_{w,T}(k) f_{cc} \left(T_{pha}(k), W_{pha}(k), m_{sa}(k), m_{w,T}(k) \right)$$

$$W_{ca}(k) = W_{pha}(k) +$$

$$(11)$$

$$m_{w,W}(k) g_{cc}(T_{pha}(k), W_{pha}(k), m_{sa}(k), m_{w,W}(k))$$
 (12)

The right hand sides of these equations are precisely the functions $f_{co}(\cdot)$ and $g_{co}(\cdot)$ in (8e)–(8f). If needed, the optimizer can choose $m_{w,W}$ to be zero while choosing a non-zero $m_{w,T}$, thus providing cooling but no dehumidification ($T_{ca} < T_{pha}$ and $W_{ca} = W_{pha}$). The flexibility due to the two fictitious water flow rates is the key for the optimizer to provide cooling without dehumidification. The equality constraint (8g) with the high penalty on the slack variable (ζ_{m_w}) ensures that the two chilled water flow rate variables are equal most of the time. The optimizer lets them take distinct values only when the mixed air conditions force the equality $W_{ca} = W_{pha}$ (i.e., no dehumidification) and high heat gain requires cooling to be provided to avoid zone temperature from exceeding the allowed range.

3.2. Model predictive controller incorporating only sensible heat (S-MPC)

Fig. 5 shows the control architecture of *S-MPC*. This controller is similar to *WISL-MPC*, with the main difference being that humidity and latent heat of air are not considered. This MPC controller is representative of the majority of MPC controllers proposed in the literature for HVAC control, e.g., [35].

As in case of the previous MPC controller, the decision variables consists of x(k), v(k), and $\zeta(k)$, which are defined as follows: $x(k) := T_{ia}(k) \in \mathbb{R}$, $v(k) := u(k) \in \mathbb{R}^5$, and $\zeta(k) := [\zeta_T^{low}(k), \zeta_T^{high}(k)] \in \mathbb{R}^2$, where

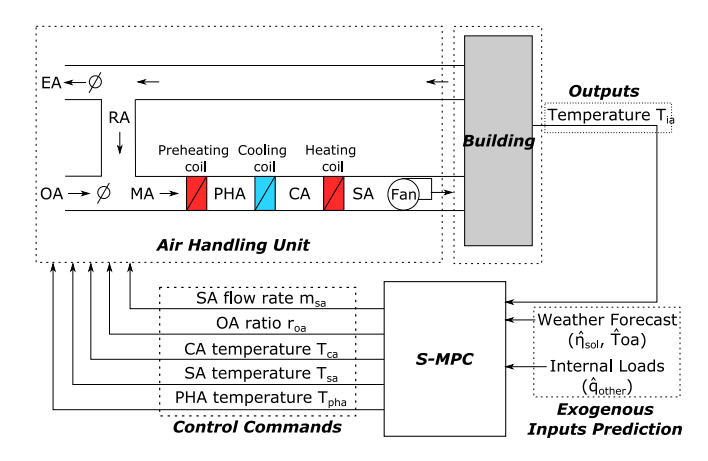


Fig. 5. S-MPC, control architecture. In this figure, OA: outdoor air, EA: exhaust air, RA: return air, MA: mixed air, PHA: preheated air, CA: conditioned air, and SA: supply air.

Table 1
Representative locations chosen for the various climate zones defined in IECC [34].

Climate zone	Location (City, County, State)	
1	Miami, Miami-Dade, Florida	
2A	Gainesville, Alachua, Florida	
2B	Tucson, Pima, Arizona	
3A	Dallas, Dallas, Texas	
3B	El Paso, El Paso, Texas	
3C	Santa Barbara, Santa Barbara, California	
4A	Washington, D.C.	
4B	Albuquerque, Bernalillo, New Mexico	
4C	Seattle, King, Washington	
5A	Chicago, Cook, Illinois	
5B	Denver, Denver, Colorado	
6A	Portland, Cumberland, Maine	
6B	Helena, Lewis and Clark, Montana	
7	Fargo, Cass, North Dakota	

u(k) is the control command vector defined in (1). The value of $\Delta t = 10$ minutes and N = 144 (corresponding to a planning horizon of 24 h), which are the same as those in *WISL-MPC*. Therefore, there are 1152 (= 144×{1 +5 +2}) decision variables.

The optimization problem at time index j is:

$$\min_{V,X,Z} \sum_{k=j}^{j+N-1} \left[P_{fan}(k) + P_{cc}^{S}(k) + P_{reheat}(k) + \lambda_{preheat} P_{preheat}(k) + P_{slack}(k) \right] \Delta t,$$
(13)

subject to the constraints: (8b), (8h), (8j)-(8n), and (8p).

In the objective function (13), P_{fan} , P_{reheat} , and $P_{preheat}$ are given by (4), (7), and (6) respectively. The cooling coil power consumption is computed based *only on sensible heat* balance:

$$P_{cc}^{S}(k) := \frac{m_{sa}(k)C_{pa}[T_{pha}(k) - T_{ca}(k)]}{\eta_{cc}COP_{c}},$$
(14)

The overall penalty on slack variables is defined as

$$P_{slack}(k) := \lambda_T^{low} \zeta_T^{low}(k) + \lambda_T^{high} \zeta_T^{high}(k)$$

The exogenous inputs needed to compute the constraints in the optimizer are: $w(k) := [\eta_{sol}(k), T_{oa}(k), q_{other}(k)]^T \in \mathbb{R}^3$.

There are five main differences when compared to WISL-MPC: (i) S-MPC does not need zone humidity measurement. (ii) The cooling power term (14) in the objective function (13) is based only on the sensible heat; latent heat is ignored. (iii) Since S-MPC does not consider humidity and latent heat, humidity constraints at various locations in the air loop as well as the zone—(8d), (8i), (8o), and (8q)—are no longer present. (iv) The cooling and dehumidifying coil model equations—(8e),

(8f), and (8g) – are also not present as constraints. (v) Prediction of the exogenous inputs W_{oa} and ω_{other} are not needed. The optimization problem in this MPC controller too is nonconvex.

3.3. Plant-model mismatch in MPC

A dynamic model used by an MPC controller appears as equality constraints in the underlying optimization problem. The hygrothermal dynamic model used by WISL-MPC is distinct from the one used by the virtual building (VB) simulator, since the former is a 2-state (1 temperature and 1 humidity) model while the latter is a 3-state (2 temperature and 1 humidity) model. There is also mismatch between the cooling coil model used by WISL-MPC and that used by the VB. The plant-model mismatch between S-MPC and the VB is even larger since S-MPC does not use a zone humidity model and does not model the change in humidity across the cooling coil. If closed loop simulations indicate that an MPC controller can maintain indoor temperature and humidity within prespecified bounds, this plant-model mismatch provide confidence in the simulation results.

3.4. Baseline controller (BL)

For the baseline, we consider the rule-based *Dual Maximum* [7] controller whose schematic representation is shown in Fig. 6. The *Dual Maximum* controller operates in three modes based on the zone temperature: (i) Cooling, (ii) Deadband, and (iii) Heating. The supply airflow rate (m_{sa}) and temperature (T_{sa}) are varied based on the mode. The controller makes decisions to change mode based on room temperature, and computes setpoints based on the mode it is in. Lower-level PI control loops are used for tracking setpoints. Time-duration based guard logic is used to prevent excessive switching of modes. The decision logic for switching modes is explained below. The reader is referred to [7] for more details about the Dual Maximum controller.

- Cooling mode: If the zone temperature is warmer than the cooling set point, the controller is in cooling mode. The supply airflow rate is varied between the minimum and cooling maximum values as needed to maintain the zone at the cooling set point.
- Deadband mode: If the zone temperature is between the heating and cooling set points, the controller is in deadband mode. The supply airflow rate is kept at the minimum and the supply air temperature is equal to the conditioned air temperature, i.e., no reheat.
- Heating mode: If the zone temperature is cooler than the heating set point, the controller is in heating mode. First, the supply air temperature is increased up to the maximum allowed value as needed, to maintain the zone temperature at the heating set point. If the zone temperature still cannot be maintained at the heating set point, the supply airflow rate is varied between the minimum and the heating maximum values.

The conditioned air temperature (T_{ca}) is kept at a constant value (typically 12.8 °C), which ensures that dry air is supplied to the building always [36]. The outdoor air ratio is varied to maintain the ventilation requirements as per ASHRAE 62.1 [33] and positive building pressurization requirements. If the mixed air temperature is too low, the preheating coil is used to bring up T_{pha} , typically to 12.8 °C (55 °F), which protects the cooling coil from freezing and getting damaged.

4. Simulation setup

4.1. Climate zones

In order to compare the performance of the three controllers as a function of climate and weather, simulations are done on the same virtual building, but by varying the geographic location. These locations are selected to represent the various climate zones in the U.S. as

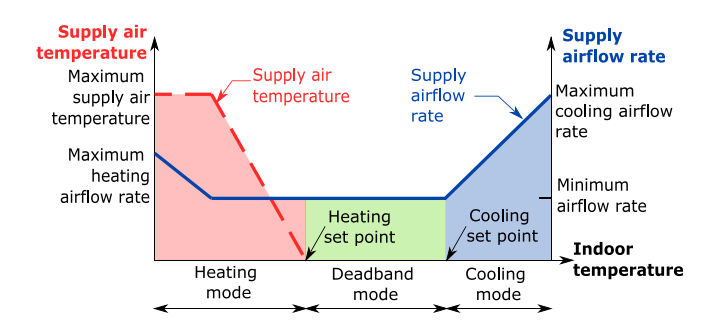


Fig. 6. Schematic of Dual Maximum control algorithm.

defined in the International Energy Conservation Code (IECC) [34]. The IECC map divides the U.S. into 8 temperature-oriented climate zones; see Fig. 7. It also divides the U.S. into 3 moisture-based climate zones: A (moist), B (dry), and C (marine) as shown in Fig. 7. In this paper, we choose 14 different locations which are listed in Table 1 and are shown as red stars in Fig. 7. The weather data for these locations are obtained from the National Solar Radiation Database (NSRDB) [37]. Climate zone 8 is not discussed in this paper because of the lack of weather data, but only a few locations fall in zone 8.

4.1.1. Choice of simulation periods

For each climate zone discussed in Section 4.1, we classify outdoor weather data into four seasons: (i) spring comprising of March, April, and May, (ii) summer comprising of June, July, and August, (iii) winter comprising of December, January, and February, and (iv) fall comprising of September, October, and November.

For each climate zone, simulations are run for four distinct weeks, each week (7 days) being representative of the corresponding season. A representative location is picked for each climate zone as described previously. For a given climate zone (thus, location) the week whose average temperature is closest to the average temperature of the entire season is chosen as the representative week for that season and for that climate zone. As an example, Fig. 8 (bottom) shows the four representative weeks of the year 2016 for climate zone 2A. The top plot of Fig. 8 zooms in to spring: the data shows that the second week is representative of spring for this particular climate zone in 2016.

Because of the way these weeks are selected, the representative week for the same season maybe distinct for distinct climate zones. Table 2 shows the start dates for these weeks for each of the climate zones.

4.2. Virtual building parameters

The parameters of the virtual building are chosen based on a large classroom/auditorium (\sim 6 m high and floor area of \sim 465 m²) in Pugh Hall located at the University of Florida, USA. We present only the relevant details here, the interested readers are referred to [4] for a complete list of the parameter values used.

The scheduled occupancy is from 7:30 AM to 7:00 PM, Monday to Friday, during which the following constraints are used: $T_{ia}^{low,occ} = 21.1$ °C (70 °F), $T_{ia}^{high,occ} = 23.3$ °C (74 °F), $RH_z^{low,occ} = 10\%$, and $RH_z^{high,occ} = 60\%$. The unoccupied hours are from 7:00 PM to 7:30 AM, Monday to Friday, and all of Saturday and Sunday, during which the following constraints are used: $T_{ia}^{low,unocc} = 18.9$ °C (66 °F), $T_{ia}^{high,unocc} = 25.6$ °C (78 °F), $RH_z^{low,unocc} = 10\%$, and $RH_z^{high,unocc} = 60\%$.

Fig. 9 shows the occupancy profile used in the simulations. q_{other} and ω_{other} are computed based on the number of occupants (n_p) in the zone, assuming that each person produces 100 W of heat and 1.39×10^{-5} kg/s (50 g/h) of water vapor [32]. For q_{other} , an additional heat load of 6000 W is considered based on lighting/equipment power density of 12.92 W/m² (1.2 W/ft²), during the scheduled occupied hours. This additional heat load is reduced to 3000 W during the unoccupied hours.

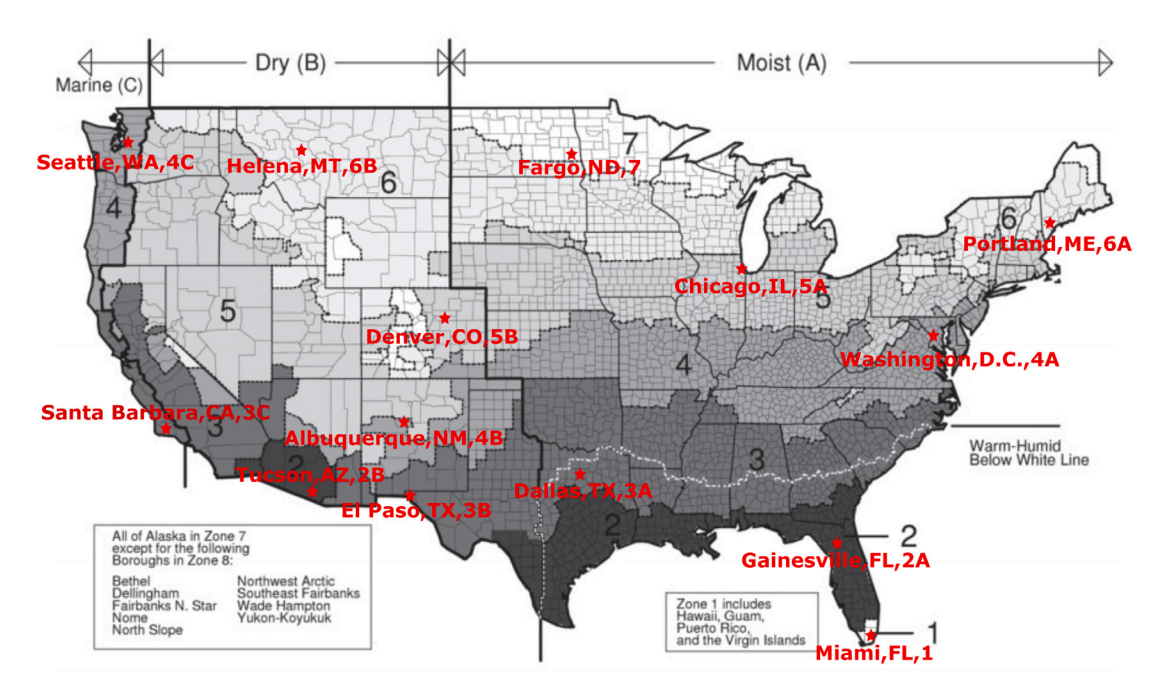


Fig. 7. Climate zones defined by IECC [34, Figure C301.1]. The representative cities chosen for each climate zone are shown as red stars. As the map legend shows, zone 7 includes most of Alaska, while Zone 1 includes Hawaii, Puerto Rico, Guam and U.S. Virgin Islands, which are not shown in the map.

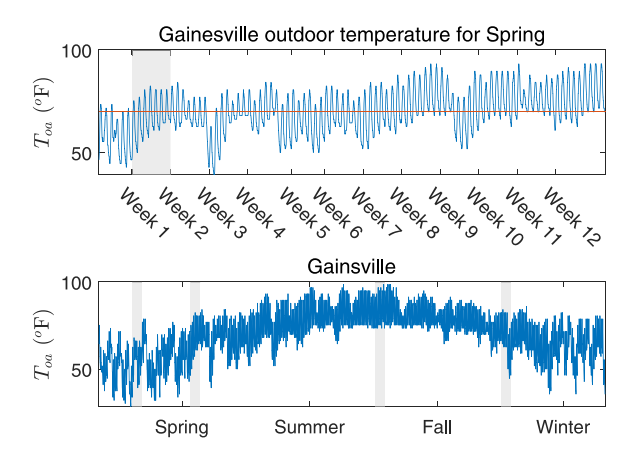


Fig. 8. Selection of representative weeks for climate zone 2A. Top: Average outdoor temperature of week 2 in spring is closest to the average temperature over all 12 weeks of spring, which is shown as the red horizontal line. (Bottom) The four representative weeks – shown as shaded bars – for the four seasons in 2016 in Gainesville, FL (climate zone 2A).

4.3. Controller parameters

MPC: The MPC controllers require prediction of exogenous inputs over the planning horizon, which is taken as 24 h (N=244) in this study. We compute the loads due to occupants in q_{other} and ω_{other} by assuming designed number of occupants (175 persons) during the scheduled occupied hours. Forecasts of remaining exogenous disturbances are assumed to be known exactly and come from weather data.

We do not assume that the building is equipped with specialized sensors, especially occupancy counters. So the minimum airflow rate is computed based on the designed number of occupants ($n_p=175$) during the scheduled occupied hours and used by the MPC controllers, so that the ventilation requirements by ASHRAE 62.1 [33] are satisfied. During unoccupied hours, the minimum allowed airflow rate is reduced to satisfy the building pressurization requirements.

For WISL-MPC , the coefficients for the convexified humidity constraint in (8i) are $a^{high}=0.000621~{\rm kg}_w/{\rm kg}_{da}/^{\rm o}{\rm C},~b^{high}=-0.173323~{\rm kg}_w/{\rm kg}_{da},~a^{low}=0.000101~{\rm kg}_w/{\rm kg}_{da}/^{\rm o}{\rm C},~{\rm and}~b^{low}=-0.028104~{\rm kg}_w/{\rm kg}_{da}.$ Fig. 10 shows the convex sets for the thermal comfort constraints which are used in WISL-MPC .

The parameters of the hygrothermal model used by the MPC controllers are specified as follows. Recall from Section 2.1.1 that a second order model of the temperature dynamics is used in the virtual building simulator, whose parameters are obtained by fitting the model's prediction to measured data. The parameters of the first order 1R-1C model used by both the MPC controllers are obtained by creating a 1R-1C approximation to the 2R-2C model in the virtual building, so that the DC gains and time constants of the transfer functions of the two models, with T_{oq} and the heat gains as inputs and the zone temperature as output, are approximately equal. The DC gain of a stable transfer function G(s), where s is the Laplace variable, is G(0), which determines the gain between a constant input and the corresponding constant steady state output [38]. The only parameter that needs to be chosen for the humidity dynamic model for WISL-MPC is the volume of the building, which was computed from architectural drawings of the auditorium of Pugh Hall.

BL parameters: The conditioned air temperature (T_{ca}) is always maintained at 12.8 °C (55 °F). The preheated air temperature is varied as follows:

$$T_{pha}(k) = \begin{cases} 12.8 \text{ °C}, & \text{if } T_{ma}(k) < 12.8 \text{ °C} \\ T_{ma}(k), & \text{otherwise.} \end{cases}$$
 (15)

The minimum outdoor airflow rate is computed in the same way as for the MPC controllers. The maximum heating airflow rate is 2.8 kg/s and the maximum cooling airflow rate is 4.6 kg/s. To ensure that the zone temperature is within the allowed comfort limits by the start of scheduled occupancy (7:30 AM), indoor temperatures constraints are changed from [18.9 °C, 25.6 °C] to [21.1 °C, 23.3 °C], 2 h prior to the start time, at 5.30 AM.

4.4. Performance metrics

We use three performance metrics to compare all three controllers: (i) the total energy consumed over a week, (ii) zone temperature violation over a week, and (iii) zone humidity violation over a week.

Table 2
Weeks for which simulations are conducted

Location (climate)	Season	Start date
Miami (1A)	Spring	14/Mar/2016
	Summer	25/Jul/2016
	Fall	31/Oct/2016
	Winter	25/Jan/2016
Gainesville (2A)	Spring	07/Mar/2016
	Summer	18/Jul/2016
	Fall	17/Oct/2016
	Winter	18/Jan/2016
Tucson (2B)	Spring	14/Mar/2016
	Summer	06/Jul/2016
	Fall	31/Oct/2016
	Winter	25/Jan/2016
Dallas (3A)	Spring	07/Mar/2016
	Summer	18/Jul/2016
	Fall	07/Nov/2016
	Winter	01/Feb/2016
El Paso (3B)	Spring	11/Apr/2016
	Summer	25/Jul/2016
	Fall	07/Nov/2016
	Winter	01/Feb/2016
	Spring	11/Apr/2016
Santa Barbara (20)	Summer	25/Jul/2016
Santa Barbara (3C)	Fall	07/Nov/2016
	Winter	25/Jan/2016
	Spring	28/Mar/2016
Westigness DC (44)	Summer	25/Jul/2016
Washington, DC (4A)	Fall	31/Oct/2016
	Winter	25/Jan/2016
Albuquerque (4B)	Spring	11/Apr/2016
	Summer	25/Jul/2016
	Fall	31/Oct/2016
	Winter	25/Jan/2016
	Spring	28/Mar/2016
Saartla (4C)	Summer	25/Jul/2016
Seattle (4C)	Fall	31/Oct/2016
	Winter	25/Jan/2016
Chicago (5A)	Spring	28/Mar/2016
	Summer	18/Jul/2016
	Fall	31/Oct/2016
	Winter	25/Jan/2016
	Spring	04/Apr/2016
D (FD)	Summer	18/Jul/2016
Denver (5B)	Fall	31/Oct/2016
	Winter	25/Jan/2016
Portland (6A)	Spring	11/Apr/2016
	Summer	18/Jul/2016
	Fall	31/Oct/2016
	Winter	25/Jan/2016
Helena (6B)	Spring	11/Apr/2016
	Summer	18/Jul/2016
	Fall	31/Oct/2016
	Winter	25/Jan/2016
	Spring	11/Apr/2016
	Summer	18/Jul/2016
		-,,
Fargo (7)	Fall	31/Oct/2016

The total energy consumed when using the controllers for a week is computed as follows:

$$E_{total} = \int_{168 \text{ h}} (P_{fan}(t) + P_{preheat}(t) + P_{cc}(t) + P_{reheat}(t)) dt,$$
 (16)

where P_{fan} , $P_{preheat}$, P_{cc} , and P_{reheat} are computed using (4), (6), (5), and (7) respectively.

The weekly zone temperature violation is computed as follows:

$$V_T = \int_{168 \, \mathrm{h}} \Delta T_{ia}(t) dt,\tag{17}$$

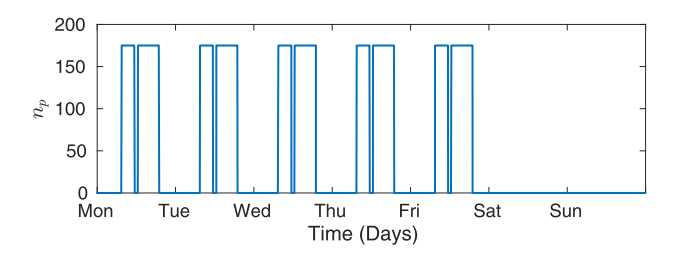


Fig. 9. Occupancy profile used in simulating the virtual building.

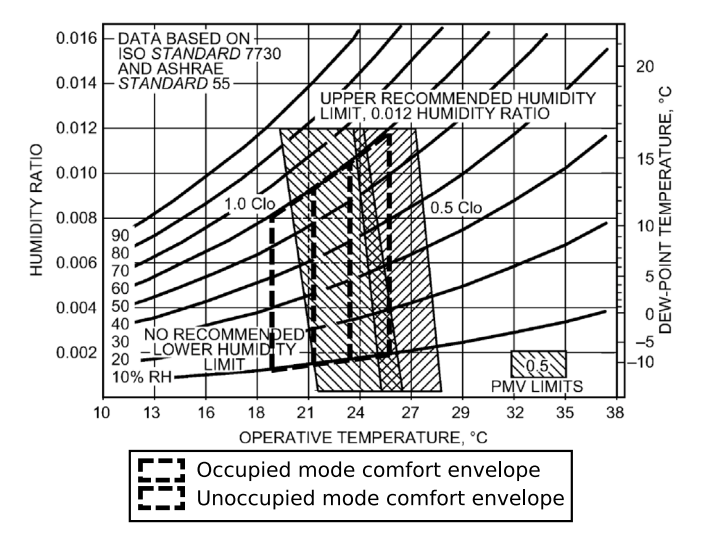


Fig. 10. Thermal comfort envelope in terms of indoor air temperature and humidity. Comfort envelope from [32] is shown as the hatched areas, and that chosen for the proposed WISL-MPC controller is shown as the shaded area during scheduled hours of occupancy and the unshaded area enclosed by dashed line during unoccupied hours.

where the term $\Delta T_{ia}(t)$ is defined as [4]:

$$\Delta T_{ia}(t) = \begin{cases} T_{ia}(t) - T_{ia}^{high}, & \text{if } T_{ia}(t) > T_{ia}^{high} \\ T_{ia}^{low} - T_{ia}(t), & \text{if } T_{ia}(t) < T_{ia}^{low} \\ 0, & \text{otherwise.} \end{cases}$$
(18)

The unit of V_T is °C-hours. Similarly, we define the weekly zone humidity violation as:

$$V_{RH} = \int_{168 \,\mathrm{h}} \Delta R H_{ia}(t) dt, \tag{19}$$

where the term $\Delta R H_{ia}(t)$ is defined as:

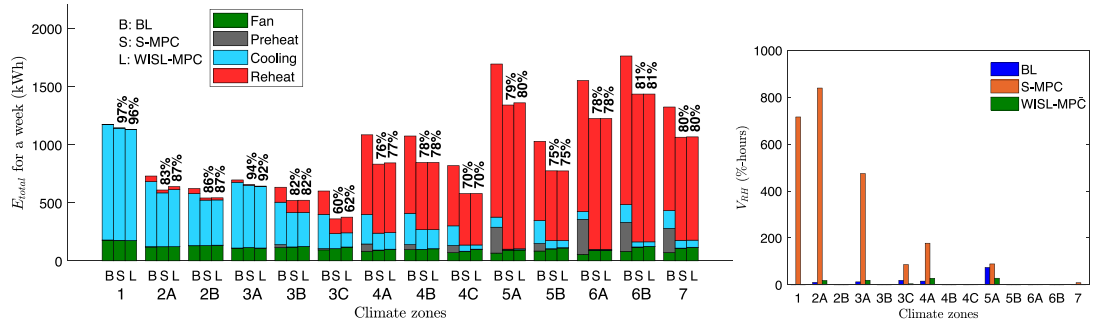
$$\Delta R H_z(t) = \begin{cases} R H_{ia}(t) - R H_{ia}^{high}, & \text{if } R H_{ia}(t) > R H_{ia}^{high} \\ R H_{ia}^{low} - R H_{ia}(t), & \text{if } R H_{ia}(t) < R H_{ia}^{low} \\ 0, & \text{otherwise.} \end{cases}$$
 (20)

The unit of V_{RH} is %-hours. The larger V_T and V_{RH} are, greater the adverse impact on occupants' comfort and health. A value of 0 is ideal.

5. Results

The simulation results for fall are found to be similar to those in spring, so we do not discuss the results for fall in the interest of space.

Real-time computation: The optimization problem within MPC - for both the MPC controllers - is solved using CasADi [39] and IPOPT [40], a nonlinear programming (NLP) solver, on a Desktop Linux computer with 16 GB RAM and a 3.60 GHZ \times 8 CPU. On average, it takes 4.48 s to solve the optimization problem in *WISL-MPC* and it takes 1.54 s to solve the optimization problem in *S-MPC* . Since the optimization problem is nonconvex for both the MPC controllers, there



- (a) Spring: Total energy consumed over a week by the three controllers by climate zone. % values refer to percentage of the baseline controller's energy consumption.
- (b) Spring: humidity violation over a week by the three controllers by climate zone. Temperature violation is essentially zero for all three controllers, and thus not presented.

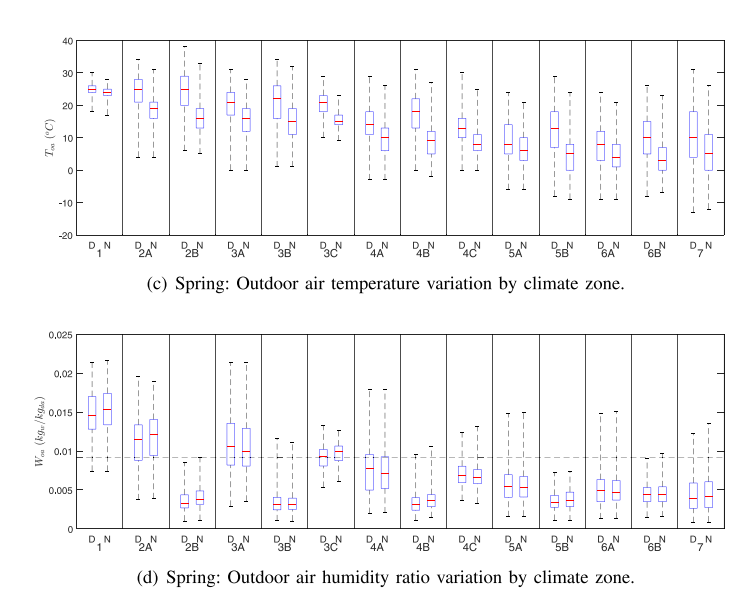


Fig. 11. Spring: Performance of the three controllers, along with statistics of outdoor weather, as a function of climate zone.

is no guarantee that the solution returned by the solver is the global minimum. Warm-start was used to help the solver find a local minimum quickly. In actual real-time implementation (as opposed to a simulation as in this case), other features can be added to help with real-time application. For instance, if the solver took more than a user-specified value to return a solution, the control command from the previously computed solution can be used. By design, the optimization problem is always feasible in both the MPC controllers due to the use of slack variables.

5.1. Results by season

The indoor air temperature violation (V_T) was found to be essentially zero for all the three controllers in all the simulations, so it is not discussed in the rest of this section.

5.1.1. Spring

Figs. 11(a) and 11(b) show the energy consumption (E_{total}) and humidity violation (V_{RH}) respectively, of each climate zone for a week in spring. The simulations results indicate the following (for spring):

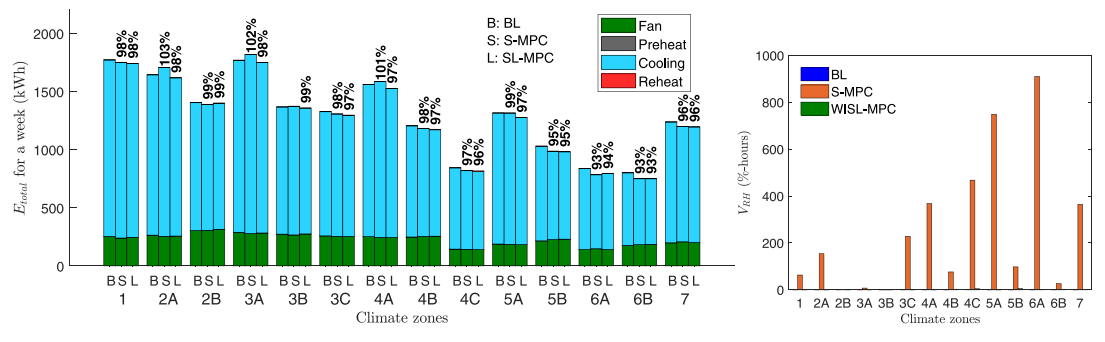
- Both WISL-MPC and BL meets indoor temperature and humidity constraints in all climate zones, but S-MPC does not: it causes large humidity violations in the warm-humid climate zones (1, 2A, and 3A).
- Both the MPC controllers have similar energy saving potential since the difference in their energy savings over BLis quite small in all climate zones.

- The energy savings from the MPC controllers over BL are substantial in all climate zones except zone 1, and vary significantly as a function of climate zone (13%–25%).
- (Not shown in plots in the interest of space) In the dry climate zones (2B, 3B, 4B, 5B, and 6B), the control commands computed by both the MPC controllers are similar. This happens since the outdoor weather is dry.

There are four main reasons MPC saves energy in comparison to BL. One, in the cold regions, WISL-MPC avoids preheating completely by recirculating as much warm air from the zone as possible. It satisfies the outdoor air requirements (m_{oa}) using a lower outdoor air ratio (r_{oa}) and a higher supply airflow rate (m_{sa}) . Whereas, BL is in the heating mode because of the somewhat cold weather in spring, so it uses a lower m_{sa} and thus a higher r_{oa} (recall that BL varies r_{oa} to maintain the minimum outdoor air requirements) to satisfy the same m_{oa} requirements. The usage of higher m_{sa} by WISL-MPC /S-MPC leads to a slightly higher fan energy consumption but a substantial decrease in the preheating energy consumption; see the results for climate zones 4A, 4B, 4C, 5A, 5B, 6A, 6B, and 7 in Fig. 11(a).

Two, BL maintains the conditioned air temperature (T_{ca}) at a constant low value of 12.8 °C (55 °F). On the other hand, WISL-MPC varies T_{ca} as long as the humidity constraints are not violated, which leads to reduction in cooling energy consumption.

Three, when the outdoor weather is pleasant (mild/cold and dry, like in climate zone 3C), MPC uses "free" cooling by bringing in more than the minimum outdoor air required which leads to further reduction in cooling energy consumption.



- (a) Summer: Total energy consumed over a week by the three controllers by climate zone. % values refer to percentage of the baseline controller's energy consumption.
- (b) Summer: Humidity violation over a week by the three controllers by climate zone. Temperature violation is essentially zero for all three controllers, and therefore not presented.

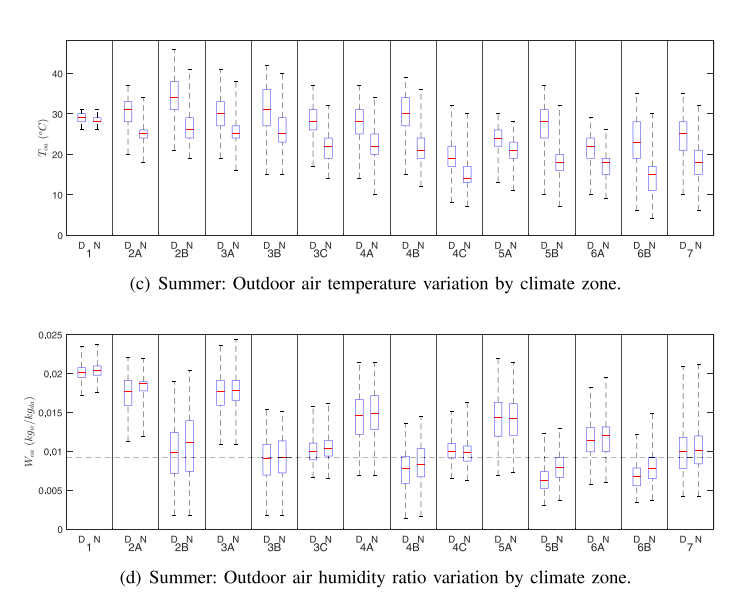


Fig. 12. Summer: Performance of the three controllers, along with statistics of outdoor weather, as a function of climate zone.

Four, BL leads to simultaneous cooling and reheating. As mentioned above, BL keeps T_{ca} at a constant low value mainly in the interest of maintaining indoor humidity [36]. Since r_{oa} is varied to bring in only the minimum amount of outdoor air needed, even if the outdoor air is moderately cold in spring, the remaining part of the mixed air which is recirculated from the zone is warm. So there is always some need for cooling. When there is not much internal heat load and the outdoor weather is cold, there is a need to reheat to maintain the zone temperature within the comfort limits. All these factors lead to cooling and reheating at the same time. On the other hand, MPC avoids this phenomenon leading to energy savings.

In the warm-humid climate zones (1, 2A, and 3A), the energy savings by WISL-MPC is moderate (4 to 13%) when compared to BL. This is mainly because of reasons two and three explained above. The scope for using free cooling is low in these climate zones as the outdoor weather is humid. Moreover, T_{ca} cannot be varied much as the humidity constraints are found to be active most of the time. In the remaining moist (type A) climate zones, and the marine (type C) climate zones, the energy savings is substantial (20% to 38%). The outdoor weather is milder and, therefore, drier, especially during nighttime in these climate zones. Therefore, there is a lot of room for optimization that WISL-MPC exploits.

The large humidity violations by *S-MPC* in the warm-humid climate zones 1, 2A, and 3A, can be attributed to two main factors. First, in an attempt to use free cooling, *S-MPC* decides to bring in more outdoor air, especially during nighttime, as the outdoor air temperature is lower than the return air. But the outdoor air is humid (which it is unaware

of). Second, *S-MPC* increases the conditioned air temperature trying to reduce cooling energy consumption. Both these factors lead to an increased supply air humidity, which in turn causes humidity constraint violations.

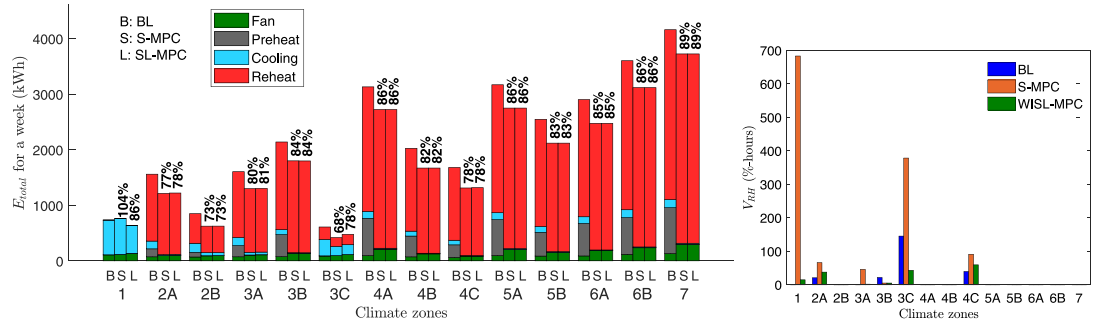
Unlike the warm-humid climate zones, the outdoor weather conditions for the remaining moist (type A) climate zones 4A, 5A, 6A, and 7, the marine (type C) climate zones 3C, and 4C are not very humid in spring; see Fig. 11(d). Therefore, the humidity violations by *S-MPC* is minimal for these zones.

Since the outdoor weather is always dry for climate zones 2B, 3B, 4B, 5B, and 6B, – see Fig. 11(d) – the control commands computed by both the MPC controllers are similar (not shown in the interest of space). The slack variable for chilled water flow rate (ζ_{m_w}) in *WISL-MPC* is found to be nonzero, i.e., $m_{w,T} \neq m_{w,W}$. This enables cooling without any dehumidification in the cooling coil, i.e., $T_{ca} \leq T_{pha}$ and $W_{ca} = W_{pha}$.

5.1.2. Summer

Figs. 12(a) and 12(b) show the simulation results for summer, which indicate the following:

• There are no humidity violations by WISL-MPC and BL, but S-MPC causes humidity violations in several climate zones. The humidity violations due to S-MPC are large in a few moist and marine climate zones (4A, 5A, 6A, 7, 3C, and 4C) but are small in the warm-humid and hot-humid climate zones (1, 2A, and 3A), but in most of climates (2A and 3A) S-MPC consumes more energy than both WISL-MPC and BL.



- (a) Winter: Total energy consumed over a week by the three controllers by climate zone. % values refer to percentage of the baseline controller's energy consumption.
- (b) Winter: Humidity violation over a week by the three controllers by climate zone. Temperature violation is essentially zero for all three controllers, and therefore not presented.

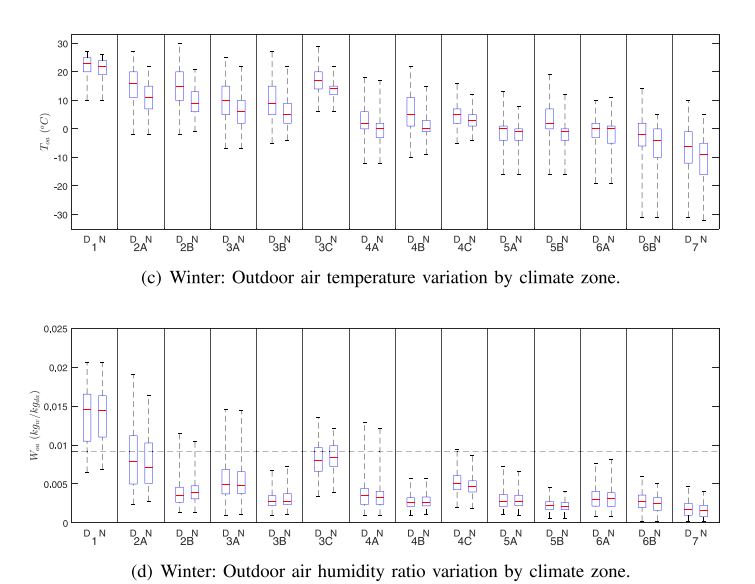


Fig. 13. Winter: Performance of the three controllers, along with statistics of outdoor weather, as a function of climate zone.

- The energy savings by both the MPC controllers over BL in all the climate zones, are small (at most 7%). In three of the warm and moist climate zones (2A, 3A and 4A), *S-MPC* consumes *more* energy than the BL.
- (Not shown in plots in the interest of space) In the dry climate zones (2B, 3B, 4B, 5B, and 6B), the control commands computed by both the MPC controllers are similar, as the outdoor weather is dry.

The reasons for small energy savings by WISL-MPC (and S-MPC) in comparison with BL are as follows. Recall that there are five control commands that a climate controller needs to decide. Since the outdoor weather is warm in most climate zones in summer, there is no preheat or reheat required, i.e., $T_{pha} = T_{ma}$ and $T_{sa} = T_{ca}$. So the controllers need to decide only the remaining three control commands: m_{sa} , r_{oa} , and T_{ca} . BL is in the cooling mode most of the time, and therefore varies m_{sa} as needed to maintain the zone temperature at the cooling set point. A similar behavior is found in WISL-MPC. Since the outdoor air temperature is warmer than the return air most of the time, WISL-MPC varies r_{oa} to bring in only the minimum outdoor air required to satisfy the ventilation and positive building pressurization requirements; this behavior is similar to BL. WISL-MPC varies T_{ca} , mainly during nighttime, while BL always maintains T_{ca} at a constant low value of 12.8 °C (55 °F). This leads to small energy savings by WISL-MPC.

The large humidity violations by *S-MPC* in climate zones 4A, 5A, 6A, 7, 3C, and 4C, can be attributed to the same two factors explained for humidity violations in the hot-humid and warm-humid climate zones (1, 2A, and 3A) during spring; see Section 5.1.1.

The humidity violations with *S-MPC* are small in the warm-humid climate zones (1, 2A, and 3A) – see Fig. 12(b) – since it decides to keep T_{ca} low In order to satisfy the high (sensible) cooling load in the building. That has an unintended, but good, side effect of maintaining indoor humidity.

In climate zones 2A and 3A, the slightly higher energy consumption by S-MPC in comparison with WISL-MPC and BL is mainly because of the following reason. During night time, S-MPC attempts to use free cooling by bringing in more outdoor air, as it is cooler than the return air from the room. But it fails to realize that the outdoor air is humid, which leads to a higher latent load on the cooling coil, and thus an increase in energy consumption.

5.1.3. Winter

Simulation results are shown in Figs. 13(a) and 13(b), which indicate the following:

- WISL-MPC and BL successfully maintain space humidity, with small humidity violation in general.S-MPC leads to large humidity violations in climate zones 1 and 3C (hot-humid and warm-humid).
- WISL-MPC leads to substantial energy savings over BL in all the climate zones (11% to 27%), and savings vary significantly by climate zone. S-MPC performs similarly to WISL-MPC in terms of energy savings, with zone 1 being an exception: S-MPC consumes more energy than BL (+4%) while WISL-MPC consumes significantly less than BL (-14%) in this zone.

 (Not presented in the interest of space) In the dry zones (2B, 3B, 4B, 5B, and 6B), the optimal control decisions made by both WISL-MPC and S-MPC are similar.

The reasons for energy savings by WISL-MPC in comparison with BL are the same as discussed in Section 5.1.1. Since the outdoor weather is cold and dry in most of the zones in winter, there is a lot of room for energy savings by appropriately varying control commands.

The higher energy use than BL and high humidity violations in the hot humid zone (zone 1) when using *S-MPC* occur because of the same reasons discussed in Section 5.1.2. Namely, *S-MPC* mistakenly believes that it can use "free cooling" from the colder outdoor air but does not recognize that humidity is not small enough to do so.

5.2. Discussion of results

The results discussed in the previous section lead to the following observations.

In all the climate zones and seasons tested, the proposed MPC controller WISL-MPC reduces energy use over BL, and it is able to maintain thermal comfort constraints as well or better than BL. The energy savings vary considerably depending on climate zone and season. Among the four seasons, summer presents the least opportunity for energy savings in every climate.

The temperature violation (V_T) was found to be nearly zero for the three controllers in all scenarios tested. The only difference was in humidity and energy consumption. The MPC scheme that ignore humidity and latent heat, S-MPC, performs close to the proposed WISL-MPC controller in both energy savings and indoor climate control in many scenarios, but with some critical exceptions. In particular, S-MPC causes humidity violations in both moist (type A) and marine (type C) climate zones, and in a subset of these scenarios, the humidity violations are quite large. Poor humidity control can not only lead to thermal discomfort of the occupants but also, in extreme cases, mold growth and associated health issues [6]. Conversely, in summer, in the climate zones in which S-MPC is able to maintain humidity well, it typically consumes more energy than even the rule-based baseline controller, though the increase is small. Even though in some scenarios, S-MPC consumes less energy than WISL-MPC, when that happens the improvement is small, about 1%-2%.

6. Conclusion

Many MPC formulations in the literature ignore humidity and latent heat considerations (i.e., dehumidification at the cooling coil). This study shows that such an MPC controller can fail to provide adequate performance – in terms of both energy use and/or humidity control – in type A (humid) and type C (marine) climate zones. The root cause of both – lack of humidity control and low energy savings (and even higher than baseline energy consumption) – is the same: the optimizer believes that there is "free cooling" from colder outdoor air while in fact the air has a high latent heat.

The primary job of an HVAC control system is to control indoor climate. High energy savings alone will not be enough for adoption of new control technologies such as MPC. The study thus confirms the need for incorporating humidity and latent heat considerations in MPC design.

Recall that the two MPC controllers studied here are designed to minimize energy use while maintaining indoor conditions: indoor temperature in case of *S-MPC* and indoor temperature and humidity in case of *WISL-MPC*. The energy consumption and indoor temperature/humidity performance of both the MPC controllers is similar in many climate zones and seasons. The difference occurs only in certain scenarios. In fact, somewhat surprisingly the MPC controller that ignores latent heat and humidity provided good indoor humidity control in hot-humid climate (zone 1) in summer. Its poor performance

occurred mostly in spring and fall in milder climates. Without this study that spans a wide range of climates and seasons, the benefit of the higher complexity MPC controller – that explicitly accounts for latent heat and humidity – would not have been clear.

This study is a first step; a more thorough assessment of costs and benefits of the two MPC formulations presented here, each with distinct levels of complexity, will require much more extensive simulations, including a study of the sensitivity to forecast errors. Although the MPC controllers in this study have significant plant-model mismatch, they have perfect prediction of thermal loads and occupancy schedules. Dependence of controller performance on the accuracy of these forecasts need to be studied carefully. Another topic for future work is to extend the current study to multi-zone buildings. Perhaps a formulation as in [41], with suitable modifications, can be used. The two MPC controllers in this paper were designed to minimize energy consumption. We suspect the effect of ignoring latent heat in the MPC formulation will be far more profound if the controller were used to provide demand-side services. This is another topic for future exploration.

CRediT authorship contribution statement

Naren Srivaths Raman: Conceptualization, Methodology, Investigation, Writing – original draft, Software. Bo Chen: Investigation, Methodology, Software. Prabir Barooah: Methodology, Supervision, Writing – original draft, Writing – review & editing.

Declaration of competing interest

The authors declare that they have no known competing financial interests or personal relationships that could have appeared to influence the work reported in this paper.

Data availability

Data will be made available on request.

References

- Serale G, Fiorentini M, Capozzoli A, Bernardini D, Bemporad A. Model predictive control (MPC) for enhancing building and HVAC system energy efficiency: Problem formulation, applications and opportunities. Energies 2018;11(3):631.
- [2] Shaikh PH, Nor NBM, Nallagownden P, Elamvazuthi I, Ibrahim T. A review on optimized control systems for building energy and comfort management of smart sustainable buildings. Renew Sustain Energy Rev 2014;34:409–29.
- [3] Pang Z, Chen Y, Zhang J, O'Neill Z, Cheng H, Dong B. Nationwide HVAC energysaving potential quantification for office buildings with occupant-centric controls in various climates. Appl Energy 2020;279:115727.
- [4] Raman NS, Devaprasad K, Chen B, Ingley HA, Barooah P. Model predictive control for energy-efficient HVAC operation with humidity and latent heat considerations. Appl Energy 2020;279:115765.
- [5] Raman NS, Chen B, Barooah P. A unified MPC formulation for control of commercial HVAC systems in multiple climate zones. In: 2020-2021 international conference on high performance buildings. West Lafayette, Indiana, USA: Purdue University: 2021.
- [6] Baughman A, Arens EA. Indoor humidity and human health–Part I: Literature review of health effects of humidity-influenced indoor pollutants. ASHRAE Trans 1996;102(Part1):192–211.
- [7] ASHRAE. The ASHRAE handbook: HVAC applications. SI ed., 2011.
- [8] Goyal S, Ingley H, Barooah P. Occupancy-based zone climate control for energy efficient buildings: Complexity vs. performance. Appl Energy 2013;106:209–21.
- [9] Rawlings JB, Mayne DQ, Diehl M. Model predictive control: theory, computation, and design. Nob Hill; 2017.
- [10] Goyal S, Barooah P. Energy-efficient control of an air handling unit for a single-zone VAV system. In: IEEE conference on decision and control. 2013, p. 4796–801.
- [11] Goyal S, Barooah P, Middelkoop T. Experimental study of occupancy-based control of HVAC zones. Appl Energy 2015;140:75–84.
- [12] Kumar M, Kar IN. Design of model-based optimizing control scheme for an air-conditioning system. HVAC R Res 2010;16(5):565–97.

- [13] Ruano AE, Pesteh S, Silva S, Duarte H, Mestre G, Ferreira PM, et al. The IMBPC HVAC system: A complete MBPC solution for existing HVAC systems. Energy Build 2016;120:145–58.
- [14] Joe J, Karava P. A model predictive control strategy to optimize the performance of radiant floor heating and cooling systems in office buildings. Appl Energy 2019;245:65–77.
- [15] Chen X, Wang Q, Srebric J. Occupant feedback based model predictive control for thermal comfort and energy optimization: A chamber experimental evaluation. Appl Energy 2016;164:341–51.
- [16] Kwak Y, Huh J-H, Jang C. Development of a model predictive control framework through real-time building energy management system data. Appl Energy 2015;155:1–13.
- [17] Yang S, Wan MP, Ng BF, Zhang T, Babu S, Zhang Z, Chen W, Dubey S. A state-space thermal model incorporating humidity and thermal comfort for model predictive control in buildings. Energy Build 2018;170:25–39.
- [18] Png E, Srinivasan S, Bekiroglu K, Chaoyang J, Su R, Poolla K. An internet of things upgrade for smart and scalable heating, ventilation and air-conditioning control in commercial buildings. Appl Energy 2019;239:408–24.
- [19] Meinrenken CJ, Mehmani A. Concurrent optimization of thermal and electric storage in commercial buildings to reduce operating cost and demand peaks under time-of-use tariffs. Appl Energy 2019:254:113630.
- [20] Zavala VM. Real-time optimization strategies for building systems. Ind Eng Chem Res 2012;52(9):3137–50.
- [21] Jiang Y, Wang X, Zhao H, Wang L, Yin X, Jia L. Dynamic modeling and economic model predictive control of a liquid desiccant air conditioning. Appl Energy 2020:259:114174.
- [22] Wang S, Jin X. Model-based optimal control of VAV air-conditioning system using genetic algorithm. Build Environ 2000;35(6):471–87.
- [23] Široký J, Oldewurtel F, Cigler J, Privara S. Experimental analysis of model predictive control for an energy efficient building heating system. Appl Energy 2011;88(9):3079–87.
- [24] Bengea SC, Kelman AD, Borrelli F, Taylor R, Narayanan S. Implementation of model predictive control for an HVAC system in a mid-size commercial building. HVAC R Res 2013:20:121–35.
- [25] Sturzenegger D, Gyalistras D, Morari M, Smith RS. Model predictive climate control of a Swiss office building: Implementation, results, and cost-benefit analysis. IEEE Trans Control Syst Technol 2016;24(1):1–12.

- [26] Yang S, Wan MP, Chen W, Ng BF, Dubey S. Model predictive control with adaptive machine-learning-based model for building energy efficiency and comfort optimization. Appl Energy 2020;271:115147.
- [27] Coffman A, Barooah P. Simultaneous identification of dynamic model and occupant-induced disturbance for commercial buildings. Build Environ 2018;128:153–60.
- [28] Goyal S, Barooah P. A method for model-reduction of nonlinear building thermal dynamics of multi-zone buildings. Energy Build 2012;47:332–40.
- [29] Raman NS, Devaprasad K, Barooah P. MPC-based building climate controller incorporating humidity. In: Proceedings of the American Control Conference, 2019, p. 253–60.
- [30] Crawley DB, Lawrie LK, Winkelmann FC, Buhl WF, Huang YJ, Pedersen CO, et al. EnergyPlus: creating a new-generation building energy simulation program. Energy Build 2001;33(4):319–31.
- [31] Raman NS, Barooah P. On the round-trip efficiency of an HVAC-based virtual battery. IEEE Trans Smart Grid 2020;11(1):403-10.
- [32] ASHRAE. The ASHRAE handbook fundamentals. SI ed., 2017.
- [33] ASHRAE. ANSI/ASHRAE standard 62.1-2016, ventilation for acceptable air quality. 2016.
- [34] International energy conservation code. International Code Council, Inc; 2018.
- [35] Ma Y, Richter S, Borrelli F. Chapter 14: Distributed model predictive control for building temperature regulation. In: Control and optimization with differential-algebraic constraints, Vol. 22. 2012, p. 293–314.
- [36] Williams J. Why is the supply air temperature 55f?. 2013, http://8760engineeringblog.blogspot.com/2013/02/why-is-supply-air-temperature-55f.html, last accessed: Aug, 03, 2020.
- [37] National solar radiation database (NSRDB). 2020, https://nsrdb.nrel.gov, last accessed: June, 01, 2020.
- [38] Ogata K. Discrete time control systems. 2nd ed.. Pearson; 1995.
- [39] Andersson JAE, Gillis J, Horn G, Rawlings JB, Diehl M. CasADi: A software framework for nonlinear optimization and optimal control. Math Program Comput 2019;11(1):1–36.
- [40] Wächter A, Biegler LT. On the implementation of an interior-point filter line-search algorithm for large-scale nonlinear programming. Math Program 2006;106(1):25–57.
- [41] Raman NS, Chaturvedi RU, Guo Z, Barooah P. Model predictive control-based hierarchical control of a multi-zone commercial HVAC system. ASME J Eng Sustain Build Cities 2021:2:021005–1–12.